Available at www.sciencedirect.com

ScienceDirect

journal homepage: www.elsevier.com/locate/he

3D CFD model of a multi-cell high-temperature electrolysis stack

*Grant Hawkes**, *James O'Brien*, *Carl Stoots*, *Brian Hawkes*

Idaho National Laboratory, PO Box 1625, MS 3870, Idaho Falls, ID 83415-3870, USA

ARTICLE INFO

Article history:
Received 22 May 2008
Received in revised form
24 November 2008
Accepted 24 November 2008
Available online 1 January 2009

Keywords:
CFD high-temperature steam electrolysis
Hydrogen production

ABSTRACT

A three-dimensional (3D) computational fluid dynamics (CFDs) electrochemical model has been created to model high-temperature electrolysis stack performance and steam electrolysis in the Idaho National Laboratory (INL) Integrated Lab Scale (ILS) experiment. The model is made of 60 planar cells stacked on top of each other operated as solid oxide electrolysis cells (SOECs). Details of the model geometry are specific to a stack that was fabricated by Ceramatec, Inc. [References herein to any specific commercial product, process, or service by trade name, trademark, manufacturer, or otherwise, does not necessarily constitute or imply its endorsement, recommendation, or favoring by the U.S. Government, any agency thereof, or any company affiliated with the Idaho National Laboratory]. and tested at INL. Inlet and outlet plenum flow and distribution are considered. Mass, momentum, energy, and species conservation and transport are provided via the core features of the commercial CFD code FLUENT. [References herein to any specific commercial product, process, or service by trade name, trademark, manufacturer, or otherwise, does not necessarily constitute or imply its endorsement, recommendation, or favoring by the U.S. Government, any agency thereof, or any company affiliated with the Idaho National Laboratory]. A solid oxide fuel cell (SOFC) model adds the electrochemical reactions and loss mechanisms and computation of the electric field throughout the cell. The FLUENT SOFC user-defined subroutine was modified for this work to allow for operation in the SOEC mode. Model results provide detailed profiles of temperature, Nernst potential, operating potential, activation over potential, anode-side gas composition, cathode-side gas composition, current density, and hydrogen production over a range of stack operating conditions. Variations in flow distribution and species concentration are discussed. End effects of flow and per-cell voltage are also considered.

1. Introduction

Increasing dependence on conventional fossil fuels along with the shrinking supply of primary energy sources has recently emphasized the need to investigate clean and efficient new energy sources. More attention is being paid to these facts now due to the growing recognition of global climate change and environmental destruction attributed to the production and utilization of fossil fuels [1]. A clean, carbon-free source of hydrogen could be implemented for purposes such as upgrading low-quality petroleum and producing synthetic liquid fuels. Hydrogen production using

* *Corresponding author*. Tel.: +1 208 526 8767.
E-mail address: grant.hawkes@inl.gov (G. Hawkes).

0360-3199/$ – see front matter © 2008 International Association for Hydrogen Energy. Published by Elsevier Ltd. All rights reserved.
doi:10.1016/j.ijhydene.2008.11.068

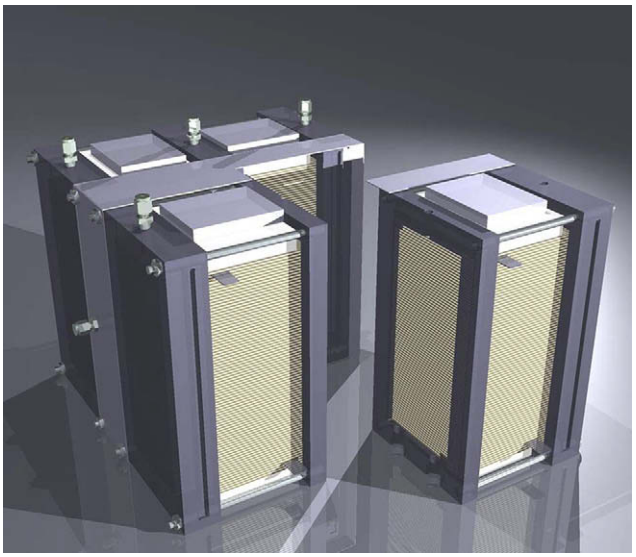

Fig. 1 – Depiction of ILS module with four 60-cell stacks with one-quarter pulled out to show what was modeled. Symmetry boundary conditions placed on inside cut-away surfaces.

a nuclear energy source would be a source of clean hydrogen [2].

Three technologies for hydrogen production using a nuclear energy source are currently being investigated in the US. According to the US Department of Energy (DOE), these processes are: high-temperature steam electrolysis (HTSE), the sulfur-iodine cycle, and the hybrid sulfur cycle [3]. The Idaho National Laboratory (INL) has been designated as the lead DOE laboratory for researching HTSE under the DOE Nuclear Hydrogen Initiative (NHI).

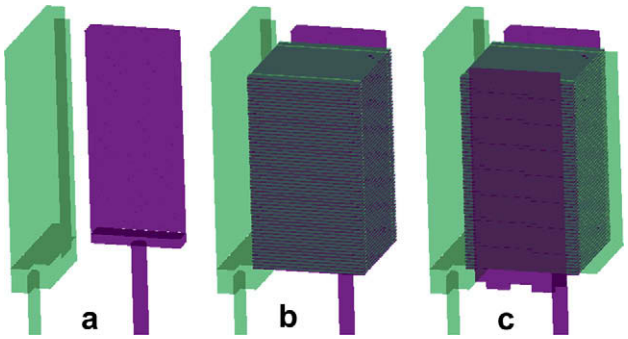

Fig. 2 – (a) Air (green) and H_2O/H_2 (purple) inlet pipe and inlet plenum (b) with current collectors added (c) with outlet plena added. [For interpretation of the references to color in this figure legend, the reader is referred to the web version of this article].

HTSE can be thought of as the reverse operation of a solid oxide fuel cell (SOFC). German researchers first investigated reversing SOFCs to produce hydrogen and oxygen with the HTSE process in the 1980s [4–6]. An HTSE research program was also begun at Riso National Laboratory in Denmark, where progress has been made from the 1990s up to the present time [7]. INL's research program began in 2003 and is intended to address simultaneously the development and scale-up of solid oxide electrolysis cell (SOEC) technology for hydrogen production from steam. This program includes an experimental component aimed at performance characterization of electrolysis cells and stacks. Results of some multi-cell tests have been documented in several recent papers [8,9]. It also includes a modeling component that seeks to understand the mechanisms governing SOEC operation. An in-depth literature search for CFD modeling of HTSE suggests

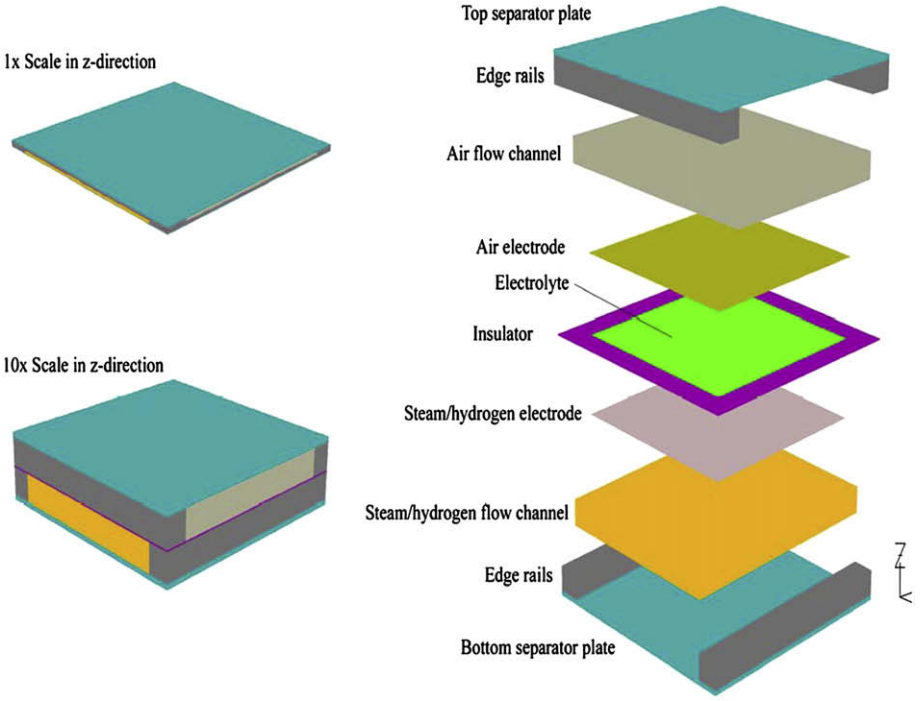

Fig. 3 – Component description for a single cell.

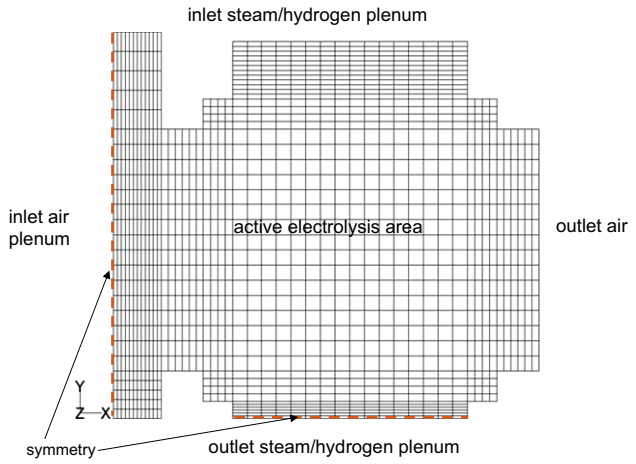

Fig. 4 – Mesh used at each cross section in z-direction.

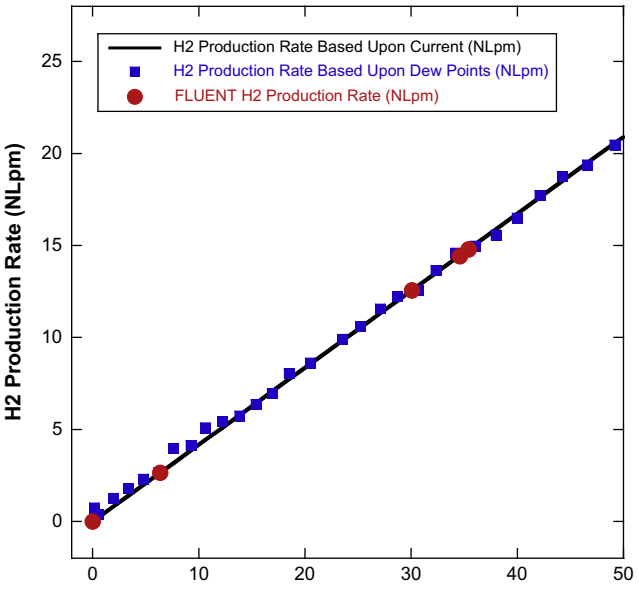

Fig. 5 – Hydrogen production rate comparison with experiment, theoretical, and FLUENT CFD.

that the author and colleagues at the INL may be the only source for these kinds of models. The specific motivation of the modeling analysis described in this paper is to understand the impact of flow distribution on the operation of the cell stack in order to optimize its performance.

This paper reports the first plenum study of a 60-cell stack simulating planar solid oxide electrolysis cells (SOEC) with the FLUENT code and SOFC module [10]. This code was used for detailed SOEC modeling. Fluent Inc. was funded by the DOE National Energy Technology Laboratory (DOE-NETL) to develop a solid oxide fuel cell (SOFC) module for coupling to the core mass, momentum, energy, and species conservation and transport features of the FLUENT computational fluid dynamics (CFD) code. The SOFC module adds the electrochemical reactions and loss mechanisms and computation of the electric field throughout the cell. The FLUENT SOFC user-defined subroutine was modified for this work to allow for operation in the SOEC mode. Model results provide detailed profiles of temperature, Nernst potential, operating potential,

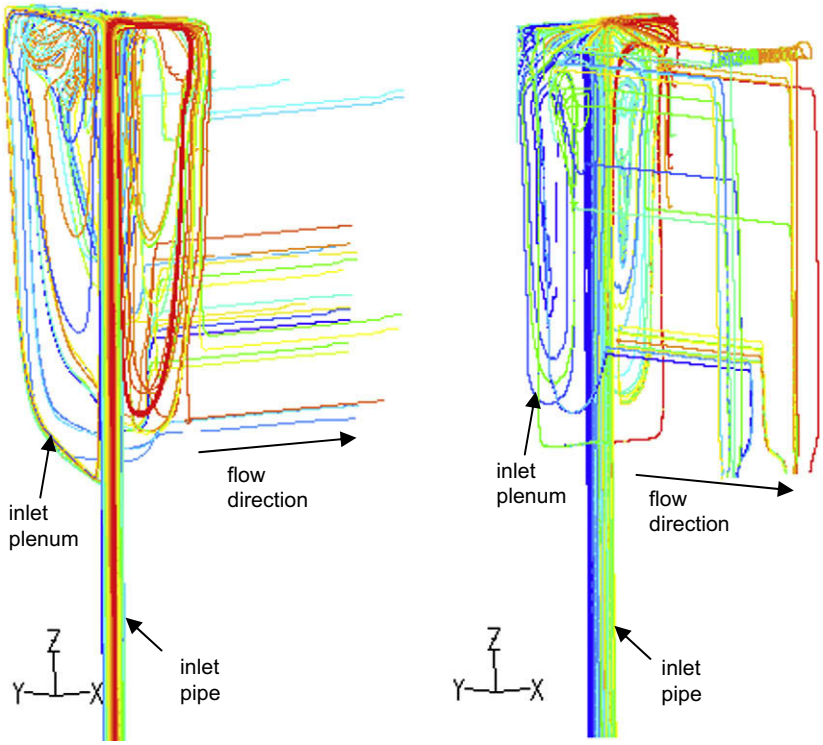

Fig. 6 – Path lines for O_2 (left) and H_2/H_2O right.

anode-side gas composition, cathode-side gas composition, current density, and hydrogen production over a range of stack operating conditions. Ref. [11] has details of the FLUENT code and numerical model. Results of the numerical model are shown in this article.

2. Numerical model

The numerical model developed for this paper was based on the geometry of a 60-cell stack fabricated by Ceramatec, Inc. and tested at INL. A depiction of four 60-cell stacks comprising an Integrated Lab Scale (ILS) module is shown in Fig. 1. Only one stack or one quarter of the module was modeled because of symmetry conditions. The modeled stack is pulled out in the figure to show what was modeled. The stack has a per-cell active area of 64 cm^2. It is designed to operate in cross flow, with the steam/hydrogen gas mixture entering the inlet manifold on the right/back in the depiction, and exiting through the outlet manifold located in the center. Air flow enters at the other center manifold (not visible in Fig. 1) and exits at the front/right where the tabs are shown directly into the furnace. The power lead attachment tabs, integral with the upper and lower interconnected plates, are also visible in the depiction.

Fig. 2 shows the sweep gas (air) and the H_2/H_2O inlet manifolds, cells, and outlet manifolds, while Fig. 3 shows a blown up view of a single cell with its components that are scaled 10x in the z-direction.

The numerical model geometry represents a complete 60-cell stack that is one-quarter of the ILS module. Symmetry boundary conditions are implemented. The numerical domain extends from the bottom of the inlet tubes to the outlet flow path of each stream. Inlet flow tubes for the H_2/H_2O and air side are modeled 5 in. below the inlet of the plenum. This distance allows the flow to develop.

The core FLUENT mass, momentum, energy, and species concentration equations are solved as normal with the basic FLUENT software. Nernst potential, activation overpotential,

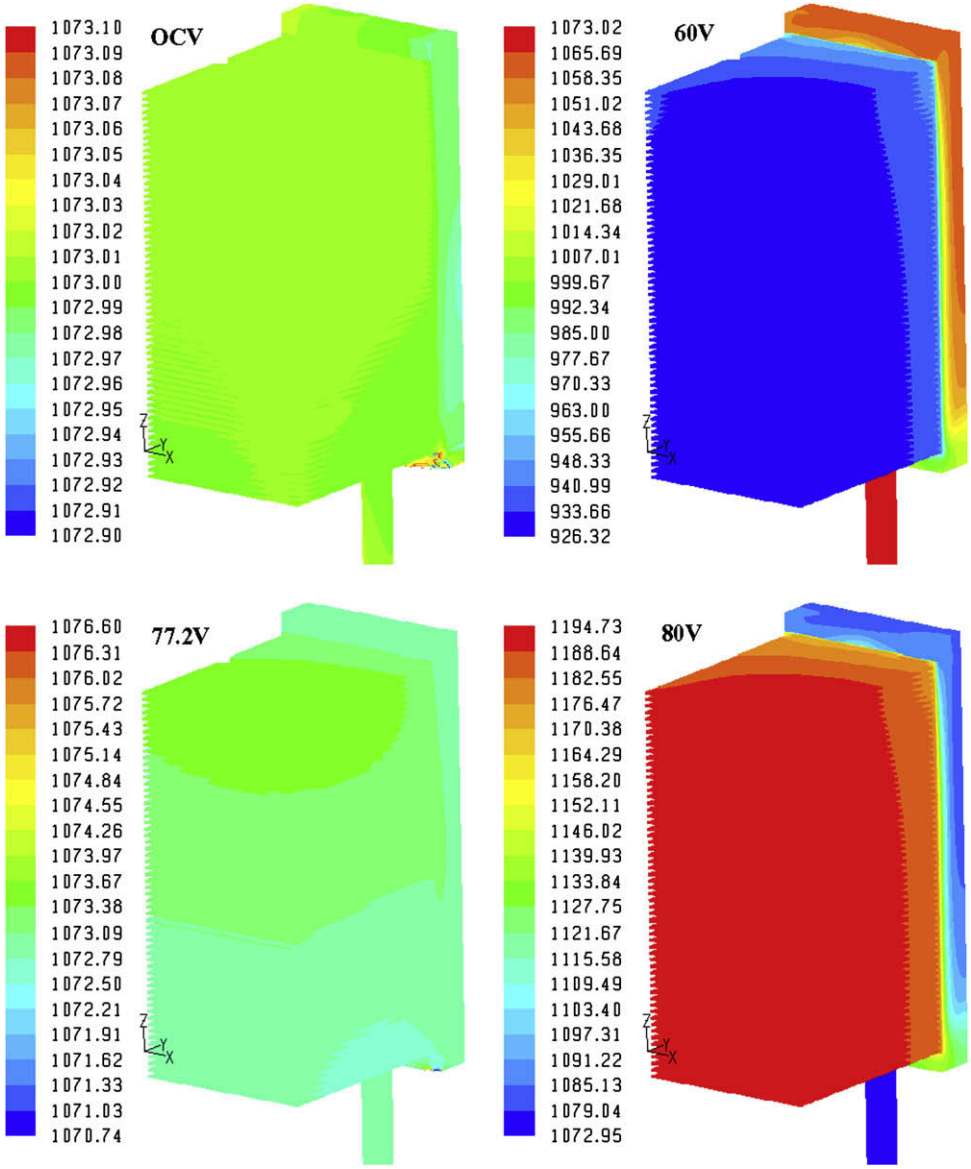

Fig. 7 – Temperature (K) contours for OCV, 60 V, 77.2 V, and 80 V.

contact resistance, conservation of current, Ohm's law, Ohmic heating, are all accounted for in the FLUENT SOFC module. The FLUENT SOFC module treats the electrolyte as a 2D planar element, meaning that the electrolyte in the model has geometrical thickness of zero. The electrolyte has a thickness of 0.14 mm. This thickness was apportioned to the separator plates so as to keep the total stack height correct. On either side of the electrolyte are the electrodes that are created with 3D elements. Therefore, the electrolyte/electrode assembly in the model is only as thick as the two electrodes.

In the electrolysis mode, the net heat flux is negative at low-current densities, where the endothermic reaction heat requirement dominates, increasing to zero at the ''thermal-neutral'' voltage, and positive at higher current densities where Ohmic heating dominates. Ohmic heating is caused by cell irreversibilities, such as electric and ionic resistance, activation, and concentration polarization. The thermal-neutral voltage can be predicted from direct application of the First Law to the overall system at a specified temperature:

$$Q - W = \dot{N}_{H_2} \Delta H_R \tag{1}$$

Letting $Q = 0$ (no external heat transfer), $W = VI$, and noting that the electrical current is directly related to the molar production rate of hydrogen by

$$\dot{N}_{H_2} = I/2F \tag{2}$$

where F is the Faraday number ($F = 96{,}487$ J/V-mol), yields:

$$V_{tn} = -\Delta H_R/2F \tag{3}$$

where V_{tn} is the thermal-neutral voltage. The open-cell potential is given by the Nernst Equation, which for the hydrogen/oxygen/steam system takes the form:

$$E = E_o - \frac{RT}{jF} \ln\left[\left(\frac{y_{H_2O}}{y_{H_2} y_{O_2}^{1/2}}\right)\left(\frac{p}{p_{std}}\right)^{-1/2}\right] \tag{4}$$

Activation overpotential due to concentration losses is not included in the FLUENT SOFC module. Mass diffusion within

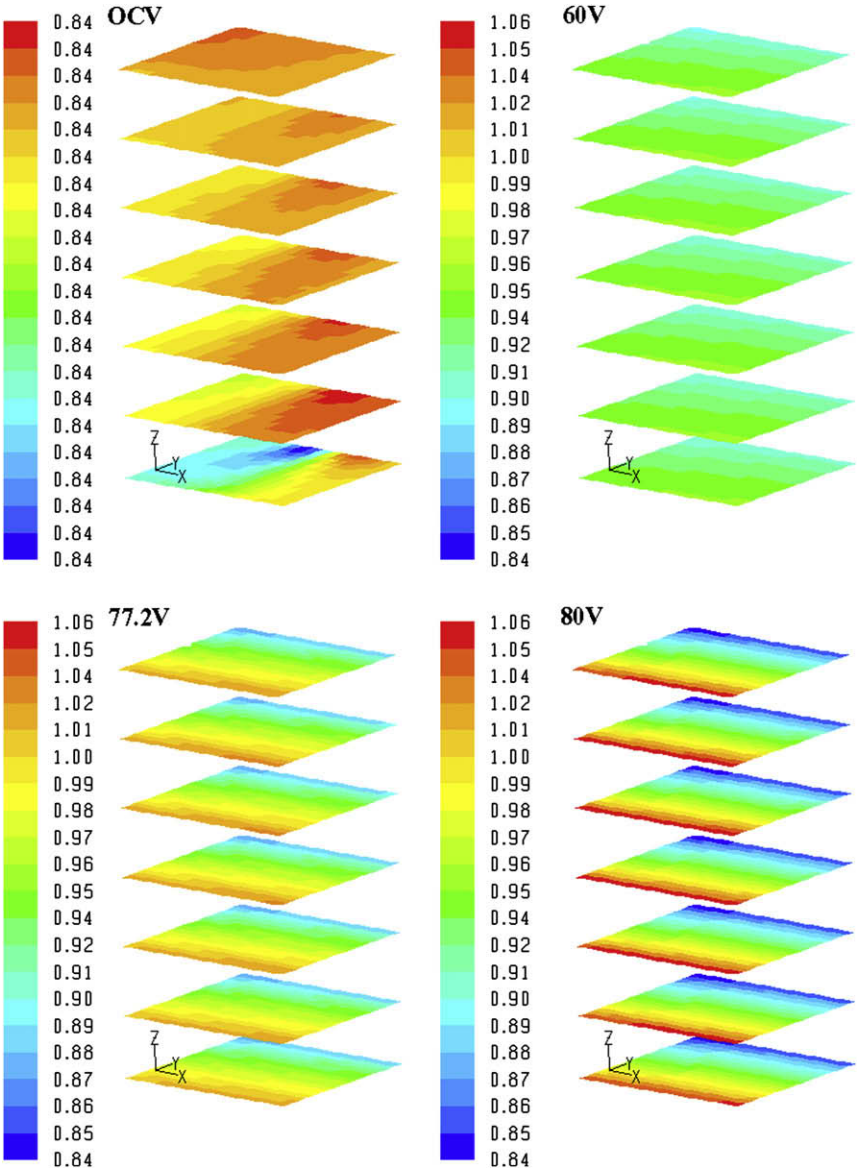

Fig. 8 – Nernst potential (V) for OCV, 60 V, 77.2 V, and 80 V.

the gas streams is calculated however. For the calculations presented, convergence was deemed acceptable after the continuity residual decreased to lower than 5×10^{-5}, which was generally achieved after about 55 iterations. The continuity residual was chosen since it always has the highest magnitude and is the slowest to converge. FLUENT was run on a double-CPU 2.6-GHz dual core machine running SUSE 10.0 Linux. With a total of 4 cpus run in parallel, each run required about 53 min of real time and 180 iterations.

Approximately 1.5 million elements are included in this model. Fig. 4 shows the top view of the grid used along with the symmetry boundary conditions. This grid was used at each level throughout the entire height of the model. The numerical grid used in this study included four elements each in the flow inlet and outlet regions, and 16×16 in the active cell area in the X and Y directions. Each flow channel (current collector) has six elements across the flow channel. Single cell numerical models with these numbers of cells give identical results to twice as many, meaning that the model is grid converged in the cell area. More research needs to be done on the mesh in the inlet and outlet plenum areas. The current collectors (flow fields) for each side are modeled as orthotropic porous media. The permeability was chosen to give the same pressure drop (12 Pa) as one dimensional frictional flow through a long thin rectangular tube described in Eq. (5):

$$\Delta P = \left(\frac{1}{2}\rho v^2\right)\left(\frac{fL}{D}\right) = \frac{\mu v L}{k} \tag{5}$$

where P is the pressure, ρ is the density, v is the velocity, f is the friction factor as a function of Reynolds number defined as 64/Re, L is the length of the cell, and D is the hydraulic diameter. The Darcy flow porous media model portion is the right side of this equation, where μ is the viscosity and k is the permeability (m^2).

All external surfaces are considered to be adiabatic. Details of the core mass, momentum, energy, and species conservation and transport features of FLUENT are documented in detail in the FLUENT user manual from Fluent Inc. Details of

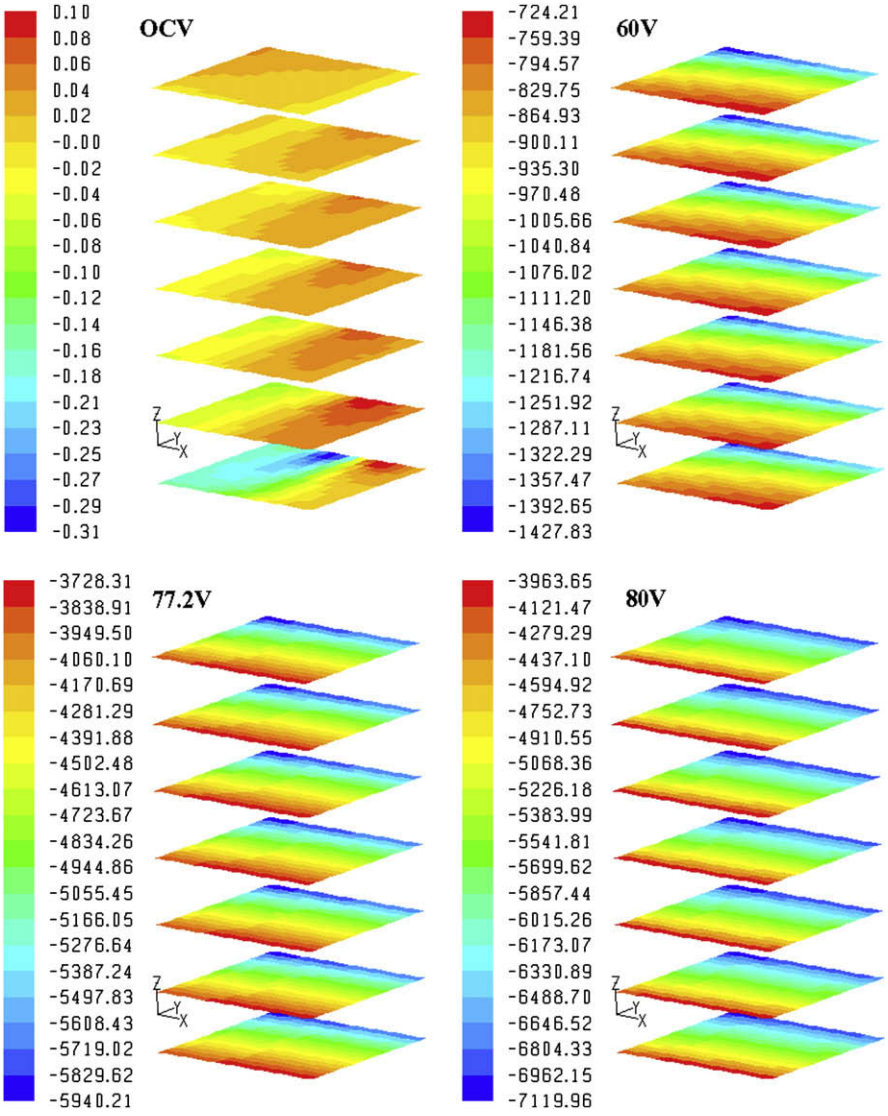

Fig. 9 – Current density (A/m^2) for OCV, 60 V, 77.2 V, and 80 V.

the electrochemical reactions, loss mechanisms, electric field computation, and electrode porous media constitutive relations are documented by the SOFC module in the FLUENT documentation. This reference also documents the treatment of species and energy sources and sinks arising from the electrochemistry at the electrode–electrolyte interfaces.

Mass flow rates for the one-quarter model were 2.18×10^{-6} kg/s and 1.83×10^{-6} kg/s for the steam/hydrogen and air flow respectively. Compositions and other parameters were taken from the base case of Ref. [12]. As a reference for comparison with experimental results, Fig. 5 shows the H_2 production rate as a function of current for the theoretical, experimental, and FLUENT results. The FLUENT results are exactly on top of the theoretical production rate of $N_{H2} = I/2F$, where N_{H2} is the molar production rate of H_2, I is the total current, and F is the Faraday constant. Reference [11] shows how the author has in the past correlated the activation overpotential, contact resistance, and other parameters to obtain the same experimental V–I curves with FLUENT. As noted in that reference, it is impossible to predict a priori the physical parameters such as contact resistance in order to match the numerically produced polarization curve with experimental results. Ref. [13] also shows the numerical reproduction of V–I curves with experimental results for electrolysis.

3. Results

Results are displayed in Figs. 6–12. Fig. 6 shows the path lines of the flow for the air inlet and H_2/H_2O inlet at open-cell voltage (OCV). Most of the flow appears to go all the way to the top of the plenum and then recirculate down the outside before entering into the various cells.

Temperature contour plots displayed on the H_2 side current collector, H_2/H_2O inlet plenum, and inlet pipe for OCV, 60 V, 77.2 V, and 80 V are shown in Fig. 7. These values correspond to 0.84, 1.0, 1.28667, and 1.333 V/cell respectively. Since the inlet temperature is at 1073 K, the thermal-neutral voltage is 1.28667 V/cell. The scale for each figure goes from the minimum to the maximum for each particular model. The top left figure is for OCV, top right is for 60 V, bottom left for

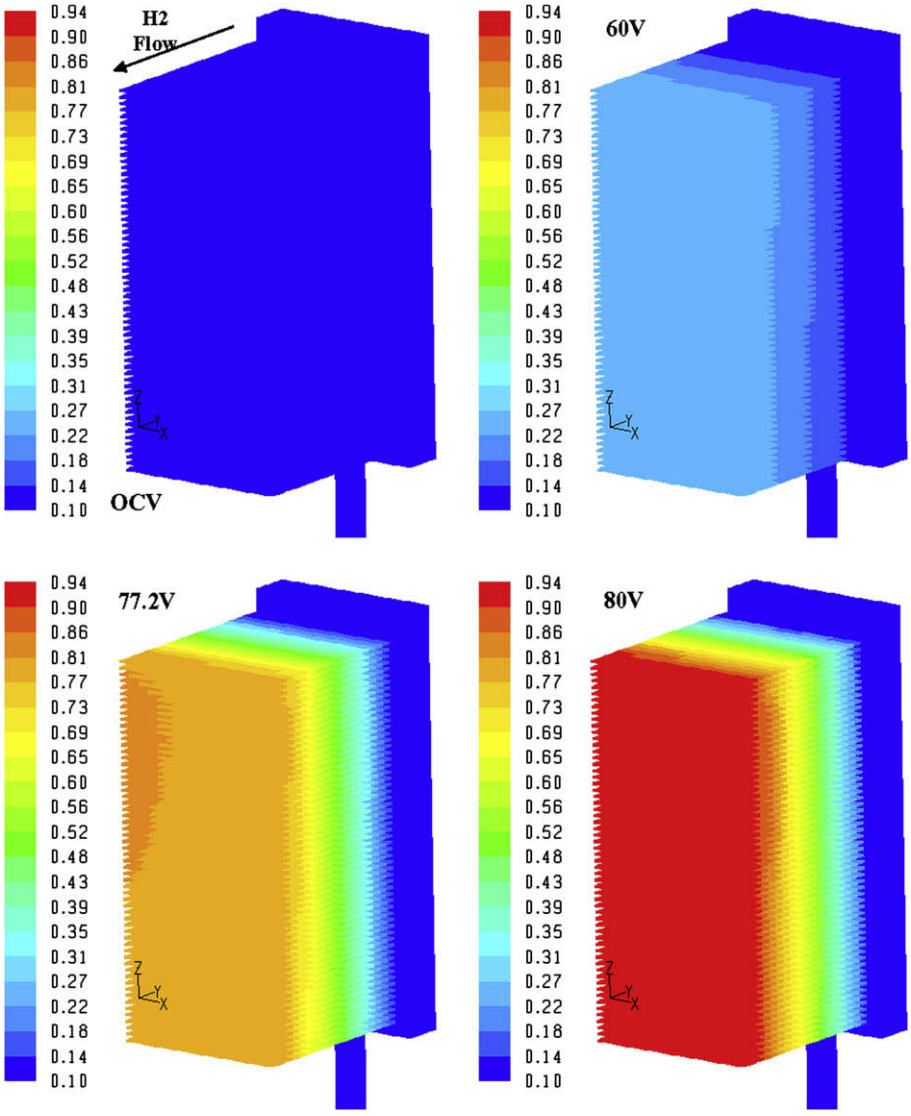

Fig. 10 – H_2 mole fraction for OCV, 60 V, 77.2 V, and 80 V.

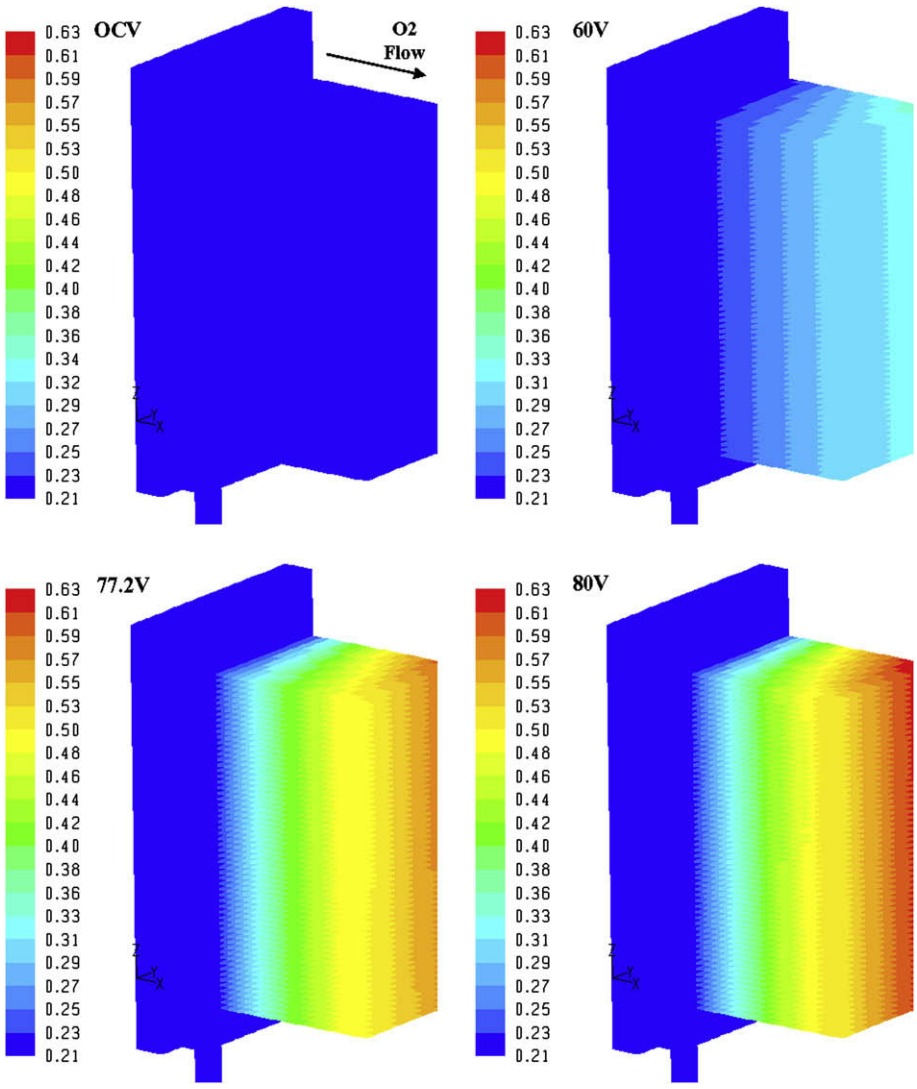

Fig. 11 – O_2 mole fraction for OCV, 60 V, 77.2 V, and 80 V.

77.2 V, and bottom right for 80 V. The 60 V figure in each set is dominated by the endothermic reaction and shows temperatures well below the inlet conditions, while the 77.2 V figure in each set has a mean outlet gas temperature exactly equal to the inlet temperature of 1073 K for the thermal-neutral case. The 80 V figure of the set shows that temperatures are dominated by the Ohmic heating in the electrolyte and well above the thermal-neutral condition.

Fig. 8 shows the Nernst potential on each tenth electrolyte for the same four operating voltages mentioned above. Nernst potential is a function of the gas compositions and temperature. The 60 V plot in Fig. 8 has a constant Nernst voltage for each electrolyte. The 60 V, 77.2 V, and 80 V plots of Fig. 8 have the same color bar legend varying from a minimum of 0.84–1.06 V. The 80 V plot has a maximum of 1.06 V because of the high H_2 concentration at the exit and high temperature. Fig. 9 shows the current density (A/m^2) on each tenth electrolyte in the stack with each individual plot going from its own minimum to maximum for the color bar legend. The highest magnitude of current density, and hence H_2 production, are the most negative (blue). The highest current density magnitude always occurs at the H_2/H_2O entrance because of the favorable Nernst conditions as discussed above. Voltage boundary conditions were set for each run at the current collector for the cases of 60, 77.2, and 80 V respectively with

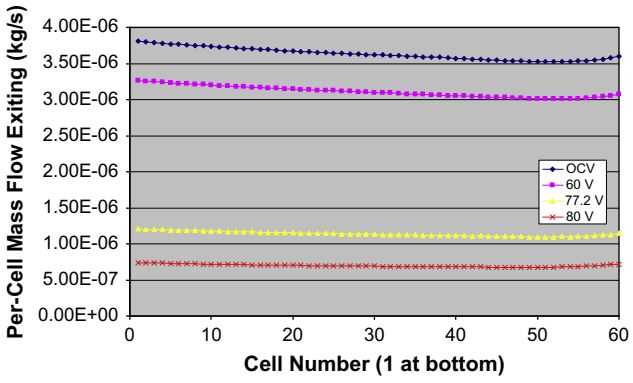

Fig. 12 – Mass flow rate exiting per cell for H_2/H_2O.

the current being calculated for each case. A very small current was set for the boundary condition for the OCV case and the voltage was calculated.

Fig. 10 shows the H_2 mole fraction in the H_2 current collector, inlet plenum, and inlet pipe. These plots show H_2 production as the flow progresses through the cells. For the plots in Fig. 10, the color bars go from the minimum observed at OCV, to the maximum mole fraction at 80 V. The thermal-neutral case at 77.2 V shows the most H_2 that is produced on the left side about 3/4 of the way up the stack. The O_2 mole fraction displayed on the O_2 current collector, and air inlet plenum and inlet pipe, is shown in Fig. 11. The amount of O_2 produced is higher near the H_2/H_2O inlet side. This is due to the high concentration of H_2O available to be electrolyzed as shown by the Nernst potential. Once again, the color bars are the same for all four plots.

Fig. 12 shows the per-cell mass flow rate exiting each cell for the H_2/H_2O and is the main basis for this study. The OCV shows the flow through the stack with no current. The flows all have the highest flow near the bottom cells and a minimum about ¾ of the way up the stack. The flow distribution is quite uniform for the highest two voltages, while a slight variation exists in the OCV and 60 V case. Previous experience shows that a mal-distribution of the flow affects the electrochemistry of the stack. The figure shows the H_2/H_2O mass flow rate is decreasing as the O_2 is produced on the O_2 electrode and flowing out with the air.

4. Conclusions

A 3D CFD model has been created to model high-temperature steam electrolysis in a planar SOEC stack. Effects of the variation of operating voltages are shown for this stack and model. The model represents a 60-cell stack that constitutes one-quarter of an ILS module. Details of the model geometry are specific to a stack that was fabricated by Ceramatec, Inc. and tested at INL. Mass, momentum, energy, and species conservation and transport are provided via the core features of the commercial CFD code FLUENT. An SOFC model adds the electrochemical reactions and loss mechanisms and computation of the electric field throughout the cell. The FLUENT SOFC user-defined subroutine was modified for this work to allow for operation in the SOEC mode. Model results provide detailed profiles of temperature, Nernst potential, operating potential, anode-side gas composition, cathode-side gas composition, current density, and hydrogen production over a range of stack operating conditions. Inlet and outlet plenums are included in the model of this stack. Plenum flow characteristics with recirculation were observed. Contour plots of local electrolyte temperature, current density, and Nernst potential indicated the effects of heat transfer, reaction cooling/heating, and change in local gas composition. A nearly uniform flow distribution in each individual cell was observed for the various operating voltages.

Acknowledgements

The US Department of Energy, Office of Nuclear Energy, Nuclear Hydrogen Initiative Program supported this work. The DOE National Energy Technology Laboratory (NETL) provided the SOFC module to the INL for this research. The Idaho National Laboratory is operated by the Battelle Energy Alliance through DOE Contract DE-AC07-05ID14517.

REFERENCES

[1] Yildiz B. Efficiency of hydrogen production systems using alternative nuclear energy technologies. International Journal of Hydrogen Energy January 2006;31(1):77–92.
[2] Forsberg CW. Hydrogen, nuclear energy, and the advanced high-temperature reactor. International Journal of Hydrogen Energy October 2003;28(10):1073–81.
[3] Henderson DA. Hydrogen production using nuclear energy. In: 2005 Annual DOE Hydrogen Program Review.
[4] Doenitz W, Schmidberger R, Steinheil E, Streicher R. Hydrogen production by high temperature electrolysis of water vapour. International Journal of Hydrogen Energy 1980;5(1):55–63.
[5] Doenitz W, Eedle E. High-temperature electrolysis of water vapor status of development and perspective for application. International Journal of Hydrogen Energy 1985;10:291–5.
[6] Doenitz W, Erdle E. High-temperature electrolysis of water vapor for hydrogen generation. International Journal of Hydrogen Energy 1982;3:29–32.
[7] Jensen M, Mogensen M. Perspectives of high temperature electrolysis using SOEC. Materials Research Department, Risø National Laboratory, DK-4000: Roskilde, Denmark.
[8] O'Brien JE, Stoots CM, Herring JS, Hartvigsen JJ. Performance of planar high-temperature electrolysis stacks for hydrogen production from nuclear energy. Nuclear Technology May, 2007;158:118–31.
[9] O'Brien JE, Stoots CM, Herring JS, Hartvigsen JJ. Hydrogen production performance of a 10-cell planar solid-oxide electrolysis stack. Journal of Fuel Cell Science and Technology May, 2006;3:213–9.
[10] FLUENT 6.3 fuel cell modules manual. Available from:. FLUENT, Inc. <www.fluent.com>; 2006.
[11] Hawkes GL, O'Brien JE, Stoots CM, Herring JS. CFD model of a planar solid oxide electrolysis cell for hydrogen production from nuclear energy. Nuclear Technology May, 2007;158:132–44.
[12] Hawkes G.L., Jones R.W. CFD Model of a Planar Solid Oxide Electrolysis Cell: Base Case and Variations. In: 2007 ASME–JSME Thermal Engineering Conference and Summer Heat Transfer Conference, Vancouver, BC, Canada; July 8–12, 2007.
[13] Herring JS, O'Brien JE, Stoots CM, Hawkes GL. Progress in high-temperature electrolysis for hydrogen production using planar SOFC technology. International Journal of Hydrogen Energy March 2007;32(4):440–50.